

Intrinsic and Extrinsic Damping in Polycrystalline Fe Thin Films

Shuang Wu,¹ David A. Smith,¹ Prabandha Nakarmi,² Anish Rai,² Michael Clavel,³ Mantu K. Hudait,³ Jing Zhao,⁴ F. Marc Michel,⁴ Claudia Mewes,² Tim Mewes,² and Satoru Emori¹

¹*Department of Physics, Virginia Polytechnic Institute and State University, Blacksburg, VA 24061, USA*

²*Department of Physics and Astronomy, The University of Alabama, Tuscaloosa, AL 35487 USA*

³*Department of Electrical and Computer Engineering, Virginia Polytechnic Institute and State University, Blacksburg, VA 24061, USA*

⁴*Department of Geosciences, Virginia Polytechnic Institute and State University, Blacksburg, VA 24061, USA*

Abstract

We examine magnetic relaxation in polycrystalline Fe films with strong and weak crystallographic texture. Out-of-plane ferromagnetic resonance (FMR) measurements reveal Gilbert damping parameters of ≈ 0.0024 for Fe films with thicknesses of 4-25 nm, regardless of their microstructural properties. The remarkable invariance with film microstructure strongly suggests that intrinsic Gilbert damping in polycrystalline Fe is a local property of nanoscale crystal grains, with limited impact from grain boundaries and film roughness. By contrast, the in-plane FMR linewidths of the Fe films exhibit distinct nonlinear frequency dependences, indicating the presence of strong extrinsic damping. To fit our experimental data, we have used a grain-to-grain two-magnon scattering model with two types of correlation functions aimed at describing the spatial distribution of inhomogeneities in the film. However, neither of the two correlation functions is able to reproduce the experimental data quantitatively with physically reasonable parameters. Our finding points to the need to further examine the fundamental impact of film microstructure on extrinsic damping.

I. INTRODUCTION

In all magnetic materials, magnetization has the tendency to relax toward an effective magnetic field. How fast the magnetization relaxes governs the performance of a variety of magnetic devices. For example, magnetization relaxation hinders efficient precessional dynamics and should be minimized in devices such as precessional magnetic random access memories, spin-torque oscillators, and magnonic circuits^{1–4}. From the technological perspective, it is important to understand the mechanisms behind magnetic relaxation in thin-film materials that comprise various nanomagnetic device applications. Among these materials, bcc Fe is a prototypical elemental ferromagnet with attractive properties, including high saturation magnetization, soft magnetism⁵, and large tunnel magnetoresistance^{6,7}. Our present study is therefore motivated by the need to uncover magnetic relaxation mechanisms in Fe thin films – particularly polycrystalline films that can be easily grown on arbitrary substrates for diverse applications.

To gain insights into the contributions to magnetic relaxation, a common approach is to examine the frequency dependence of the ferromagnetic resonance (FMR) linewidth. The most often studied contribution is viscous Gilbert damping^{8–13}, which yields a linear increase in FMR linewidth with increasing precessional frequency. In ferromagnetic metals, Gilbert damping arises predominately from “intrinsic” mechanisms^{14–16} governed by the electronic band structure¹⁷. Indeed, a recent experimental study by Khodadadi *et al.*¹⁸ has shown that intrinsic, band-structure-based Gilbert damping dominates magnetic relaxation in high-quality crystalline thin films of Fe, epitaxially grown on lattice-matched substrates. However, it is yet unclear how intrinsic damping is impacted by the microstructure (e.g., crystallographic texture) of polycrystalline Fe films.

Microstructural disorder in polycrystalline Fe films can also introduce *extrinsic* magnetic relaxation. A well-known extrinsic relaxation mechanism is two-magnon scattering, where the uniform precession mode with zero wave vector scatters into a degenerate magnon mode with a finite wave vector^{19–22}. Two-magnon scattering generally leads to a nonlinear frequency dependence of the FMR linewidth, governed by the nature of magnon scattering centers at the surfaces^{23,24} or in the bulk of the film^{25–28}. While some prior experiments point to the prominent roles of extrinsic magnetic relaxation in polycrystalline ferromagnetic films^{29–31}, systematic studies of extrinsic relaxation (e.g., two-magnon scattering) on

polycrystalline Fe thin films are still lacking.

Here, we investigate both the intrinsic and extrinsic contributions to magnetic relaxation at room temperature in polycrystalline Fe films. Specifically, we examine two series of samples: smooth Fe films with strong out-of-plane (110) texture, and rough Fe films with weak out-of-plane (110) texture. We have measured the frequency dependence of the FMR linewidth with (1) the film magnetized out-of-plane (OOP), where two-magnon scattering is suppressed²⁵ such that intrinsic Gilbert damping is quantified reliably, and (2) the film magnetized in-plane (IP), where two-magnon scattering is generally expected to coexist with intrinsic Gilbert damping. From OOP FMR results, we find that the intrinsic damping of polycrystalline Fe films is independent of their structural properties and almost identical to that of epitaxial films. This result suggests that intrinsic Gilbert damping is a local property of the metal, primarily governed by the nanoscale crystal grains rather than grain boundaries or film roughness. By contrast, the frequency dependence of IP FMR linewidth exhibits strong nonlinear trends that differ significantly between the strongly and weakly textured Fe films. To analyze the nonlinear trends, we have employed the grain-to-grain two-magnon scattering model developed by McMichael and Krivosik²⁵ with two types of correlation functions for capturing inhomogeneities in the film. However, neither of the correlation functions yields quantitative agreement with the experimental results or physically consistent, reasonable parameters. This finding implies that a physical, quantitative understanding of extrinsic magnetic relaxation requires further corrections of the existing two-magnon scattering model, along with much more detailed characterization of the nanoscale inhomogeneities of the magnetic film. Our study stimulates opportunities for a deeper examination of fundamental magnetic relaxation mechanisms in structurally disordered ferromagnetic metal films.

II. FILM DEPOSITION AND STRUCTURAL PROPERTIES

Polycrystalline Fe thin films were deposited using DC magnetron sputtering at room temperature on Si substrates with a native oxide layer of SiO₂. The base pressure of the chamber was below 1×10^{-7} Torr and all films were deposited with 3 mTorr Ar pressure. Two sample series with different seed layers were prepared in our study: subs./Ti(3 nm)/Cu(3 nm)/Fe(2-25 nm)/Ti(3 nm) and subs./Ti(3 nm)/Ag(3 nm)/Fe(2-25 nm)/Ti(3 nm). In this

paper we refer to these two sample series as Cu/Fe and Ag/Fe, respectively. The layer thicknesses are based on deposition rates derived from x-ray reflectivity (XRR) of thick calibration films. The Ti layer grown directly on the substrate ensures good adhesion of the film, whereas the Cu and Ag layers yield distinct properties for Fe as described below.

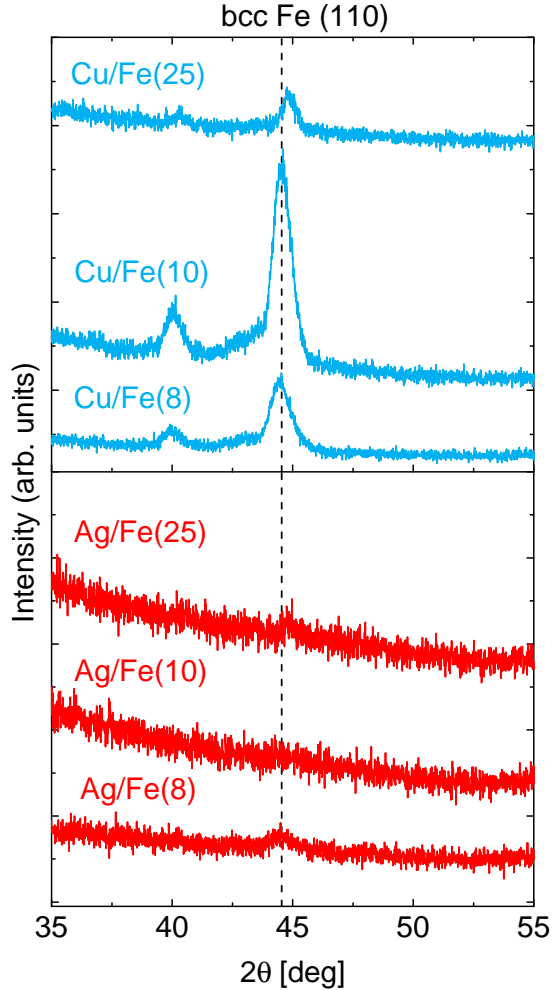


FIG. 1. (Color online) θ - 2θ X-ray diffraction scan curves of 8 nm, 10 nm, and 25 nm thick films from both Cu/Fe (blue lines) and Ag/Fe (red lines) sample series. The peak at $2\theta \approx 40^\circ$ seen for each Cu/Fe sample is attributed to the Cu K β radiation.

We performed x-ray diffraction (XRD) measurements to compare the structural properties of the Cu/Fe and Ag/Fe films. Figure 1 shows symmetric θ - 2θ XRD scan curves of 8 nm, 10 nm, and 25 nm thick films from both the Cu/Fe and Ag/Fe sample series. The (110) body-centered-cubic (bcc) peak can be observed for all Cu/Fe films around 44° . By contrast, this peak is absent or extremely weak for all Ag/Fe films. The lack of pronounced peaks in the

symmetric θ - 2θ scans does not necessarily signify that Ag/Fe is amorphous. This is because symmetric θ - 2θ XRD is sensitive to planes that are nearly parallel to the sample surface, such that the diffraction peaks capture only the out-of-plane crystallographic orientation of the film. In fact, from *asymmetric* grazing-incidence XRD scans that are sensitive to other planes, we are able to observe a bcc Fe (110) diffraction peak for Ag/Fe. We therefore deduce that both Cu/Fe and Ag/Fe are polycrystalline, with grain size on the order of film thickness estimated from the diffraction peak width via the Scherrer equation. Nevertheless, the two series are distinct in that Cu/Fe is strongly textured out-of-plane (i.e., the Fe grains are predominantly (110)-oriented out-of-plane) and Ag/Fe is weakly textured out-of-plane.

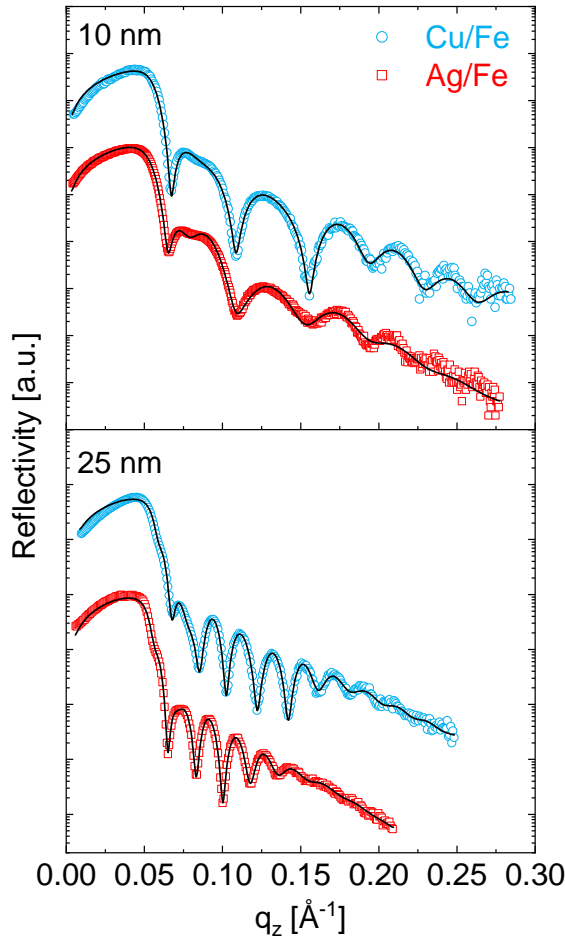


FIG. 2. (Color online) X-ray reflectivity scans of 10 nm, and 25 nm thick films from both Cu/Fe (blue open circles) and Ag/Fe (red open squares) sample series. Black solid curves are fits to the data.

We also observe a notable difference in film roughness between Cu/Fe and Ag/Fe, as

revealed by XRR scans in Fig. 2. The oscillation period depends inversely on the film thickness. The faster decay of the oscillatory reflectivity signal at high angles for the Ag/Fe films indicates that the Ag/Fe films have rougher interfaces compared to the Cu/Fe films. By fitting the XRR results³², we estimate an average roughness of $\lesssim 1$ nm for the Fe layer in Cu/Fe, while the average roughness in Ag/Fe films is much greater at $\approx 2\text{-}3$ nm³³. Thus, we conclude that Fe grown on Cu is strongly textured and smooth, whereas Fe on Ag is weakly textured and rough. Although identifying the origin of this structural difference is beyond the scope of this work, Cu/Fe and Ag/Fe constitute two qualitatively distinct series of polycrystalline Fe films for exploring the influence of microstructure on magnetic relaxation.

III. INTRINSIC GILBERT DAMPING PROBED BY OUT-OF-PLANE FMR

Having established the difference in structural properties between Cu/Fe and Ag/Fe, we characterize intrinsic damping for these samples with OOP FMR measurements. The OOP geometry suppresses two-magnon scattering²⁵ such that the Gilbert damping parameter can be quantified in a straightforward manner. We use a W-band shorted waveguide in a superconducting magnet, which permits FMR measurements at high fields ($\gtrsim 4$ T) that completely magnetize the Fe films out of plane. The details of the measurement method are found in Refs.^{18,34}. Figure 3(a) shows the frequency dependence of half-width-at-half-maximum (HWHM) linewidth ΔH_{OOP} for selected thicknesses from both sample series. The linewidth data of 25 nm thick epitaxial Fe film from a previous study¹⁸ is plotted in Fig. 3 (a) as well. The intrinsic damping parameter can be extracted from the linewidth plot using

$$\Delta H_{\text{OOP}} = \Delta H_0 + \frac{2\pi}{\gamma} \alpha_{\text{OOP}} f, \quad (1)$$

where ΔH_0 is the inhomogeneous broadening, $\gamma = \frac{g\mu_B}{\hbar}$ is the gyromagnetic ratio ($\gamma/2\pi \approx 2.9$ MHz/Oe, obtained from the frequency dependence of resonance field³⁴), and α_{OOP} is the measured viscous damping parameter. In general, α_{OOP} can include not only intrinsic Gilbert damping, parameterized by α_{int} , but also eddy-current, radiative damping, and spin pumping contributions³⁵, which all yield a linear frequency dependence of the linewidth. Damping due to eddy current is estimated to make up less than 10% of the total measured damping parameter³⁴ and is ignored here. Since we used a shorted waveguide in our setup,

the radiative damping does not apply here. Spin pumping is also negligible for most of the samples here because the materials in the seed and capping layers (i.e., Ti, Cu, and Ag) possess weak spin-orbit coupling and are hence poor spin sinks³¹. We therefore proceed by assuming that the measured OOP damping parameter α_{OOP} is equivalent to the *intrinsic* Gilbert damping parameter.

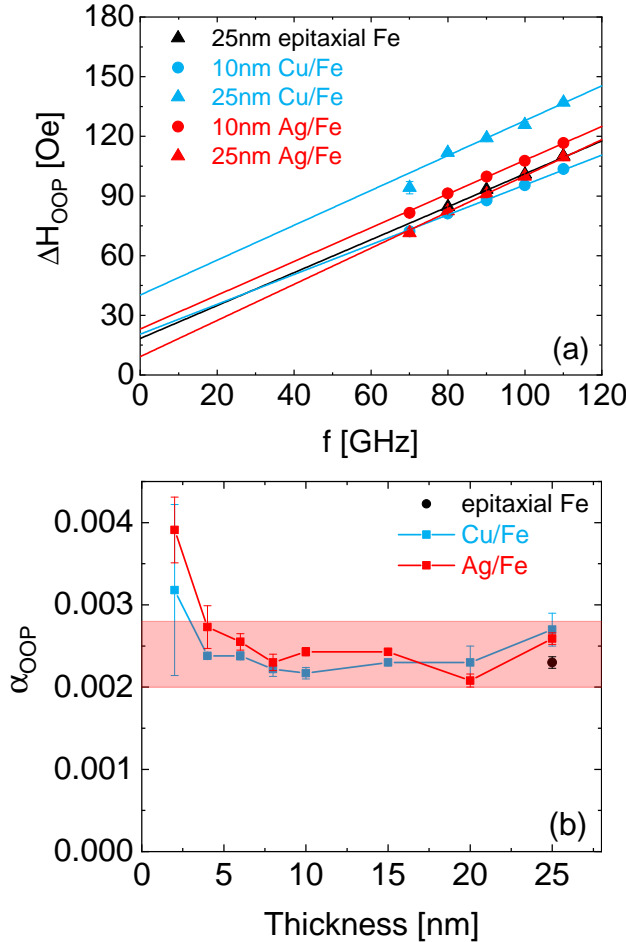


FIG. 3. (Color online) (a) OOP FMR half-width-at-half-maximum linewidth as a function of resonance frequency f . Lines correspond to fits to the data. (b) Gilbert damping extracted from OOP FMR as a function of film thickness. The red shaded area highlights the damping value range that contains data points of all films thicker than 4 nm. The data for the epitaxial Fe sample (25 nm thick Fe grown on MgAl_2O_4) are adapted from Ref.¹⁸.

The extracted damping parameter is plotted as a function of Fe film thickness in Fig. 3(b). The damping parameters of all Fe films with thicknesses of 4-25 nm fall in the range of 0.0024 ± 0.0004 , which is shaded in red in Fig. 3(b). This damping parameter range is

quantitatively in line with the value reported for epitaxial Fe (black symbol in Fig. 3(b))¹⁸. For 2 nm thick samples, the damping parameter is larger likely due to an additional interfacial contribution^{36,37} – e.g., possibly finite spin pumping that becomes nonnegligible only in ultrathin Fe. The results in Fig. 3(b) therefore indicate that the structural properties in the *bulk* of polycrystalline bcc Fe films (i.e., $\gtrsim 4$ nm thick) have little influence on their intrinsic damping.

It is remarkable that these polycrystalline Cu/Fe and Ag/Fe films – with significantly different degrees of out-of-plane crystallographic texture and film roughness (as revealed in Sec. II) – exhibit essentially the same intrinsic Gilbert damping parameter as single-crystalline bcc Fe. In the following, we discuss potential reasons as to why intrinsic damping is insensitive to the microstructure of the Fe films.

We first note that intrinsic Gilbert damping in ferromagnetic metals is predominantly governed by transitions of spin-polarized electrons between electronic states, within a given electronic band (intraband scattering) or in different electronic bands (interband scattering) near the Fermi level¹⁵. From Refs.^{18,38}, we deduce that interband scattering is dominant at room temperature in Fe. According to our results (Fig. 3(b)), such intrinsic damping from electronic transitions is evidently unaffected by the variation in the structural properties of the Fe films. A plausible explanation is that the observed intrinsic damping is mostly governed by the electronic band structure *within the Fe grains*, such that any disorder in grain boundaries has minimal impact. Electronic scattering due to grain boundaries or rough film interfaces might not significantly affect intrinsic Gilbert damping, if the relevant electron scattering is dominated by phonons within the crystal grains of Fe. In other words, the robust consistency of α_{OOP} (Fig. 3(b)) could be an indication that the intrinsic Gilbert damping parameter is a local property of the ferromagnetic metal, possibly averaged over the ferromagnetic exchange length of just a few nm³⁹ that is comparable or smaller than the grain size. In this scenario, the impact on damping from grain boundaries would be limited in comparison to the contributions to damping within the grains.

Moreover, the distribution of orientations among Fe grains – i.e., the texture of the film – evidently does not have much influence on the intrinsic damping. This is reasonable considering that intrinsic Gilbert damping is predicted to be nearly isotropic in Fe at sufficiently high electron-lattice scattering rates⁴⁰ – e.g., $\sim 10^{14}$ s⁻¹ at room temperature where interband scattering is expected to be dominant^{18,38}. Strain in Fe grains is also not expected to

impact the intrinsic damping, as Ref.¹⁸ suggests that strain in bcc Fe does not significantly alter the band structure near the Fermi level. Thus, polycrystalline Fe films exhibit essentially the same magnitude of intrinsic Gilbert damping as epitaxial Fe, as long as the grains retain the bcc crystal structure.

The observed invariance of intrinsic damping here is quite different from the recent study of polycrystalline Co₂₅Fe₇₅ alloy films³¹, reporting a decrease in intrinsic damping with increasing in structural disorder. This inverse correlation between intrinsic damping and disorder in Ref.³¹ is attributed to the dominance of intraband scattering, which is inversely proportional to the electronic scattering rate. It remains an open challenge to understand why the intrinsic Gilbert damping of some ferromagnetic metals might be more sensitive to structural disorder than others.

IV. EXTRINSIC MAGNETIC RELAXATION PROBED BY IN-PLANE FMR

Although we have shown via OOP FMR in Sec. III that intrinsic Gilbert damping is essentially independent of crystallographic texture in Fe films, it might be expected that microstructure has a pronounced impact on *extrinsic* magnetic relaxation driven by two-magnon scattering, which is generally present in IP FMR. IP magnetized films are more common in device applications than OOP magnetized films, since the shape anisotropy of thin films tends to keep the magnetization in the film plane. What governs the performance of such magnetic devices, for example the effective loss (or the inverse of the quality factor)^{41,42} may not be the intrinsic Gilbert damping parameter but the total FMR linewidth. Thus, for many magnetic device applications, it is essential to understand the contributions to the IP FMR linewidth.

IP FMR measurements have been performed using a coplanar-waveguide-based spectrometer, as detailed in Refs.^{18,34}. Examples of the frequency dependence of IP FMR linewidth are shown in Fig. 4. In contrast to the linear frequency dependence that arises from intrinsic Gilbert damping in Fig. 3(a), a nonlinear hump is observed for most of the films between 6 and 20 GHz. In some films, e.g., 10 nm thick Cu/Fe film, the hump is so large that its peak even exceeds the linewidth at the highest measured frequency. Similar nonlinear IP FMR linewidth behavior has been observed in Fe alloy films⁴³ and epitaxial Heusler films⁴⁴ in previous studies, where two-magnon scattering has been identified as a significant contributor

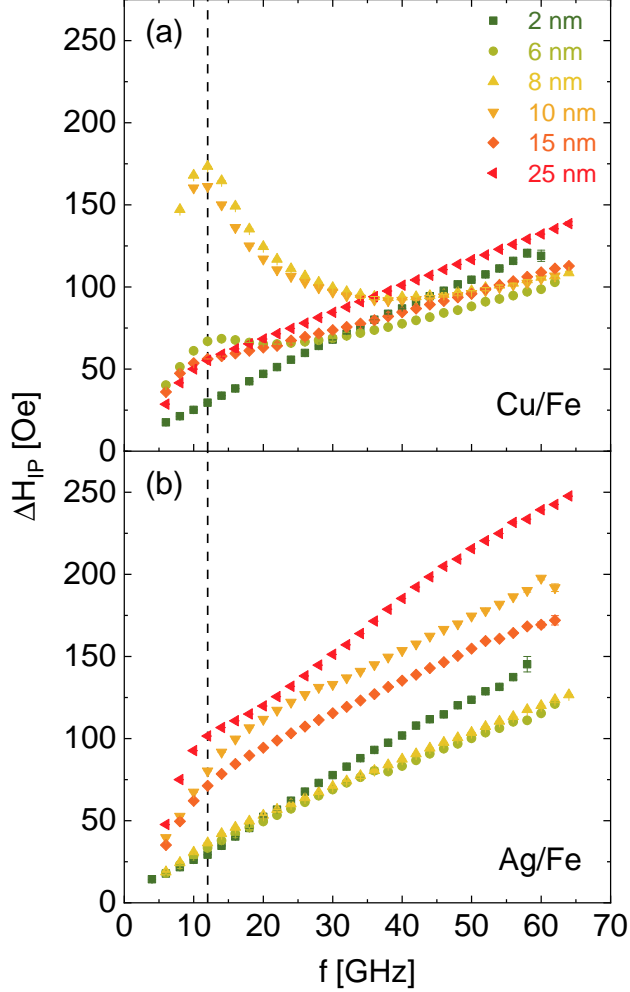


FIG. 4. (Color online) IP FMR half-width-at-half-maximum linewidth as a function of resonance frequency f for (a) Cu/Fe and (b) Ag/Fe.

to the FMR linewidth. Therefore, in the following, we attribute the nonlinear behavior to two-magnon scattering.

To gain insight into the origin of two-magnon scattering, we plot the linewidth at 12 GHz – approximately where the hump is seen in Fig. 4 – against the Fe film thickness in Fig. 5(a). We do not observe a monotonic decay in the linewidth with increasing thickness that would result from two-magnon scattering of interfacial origin⁴⁵. Rather, we observe a non-monotonic thickness dependence in Fig. 5(a), which indicates that the observed two-magnon originates within the bulk of the films. We note that Ag/Fe with higher film roughness (see Sec. II) exhibits weaker two-magnon scattering than Cu/Fe, particularly in the lower thickness regime ($\lesssim 10$ nm). This observation further corroborates that the two-

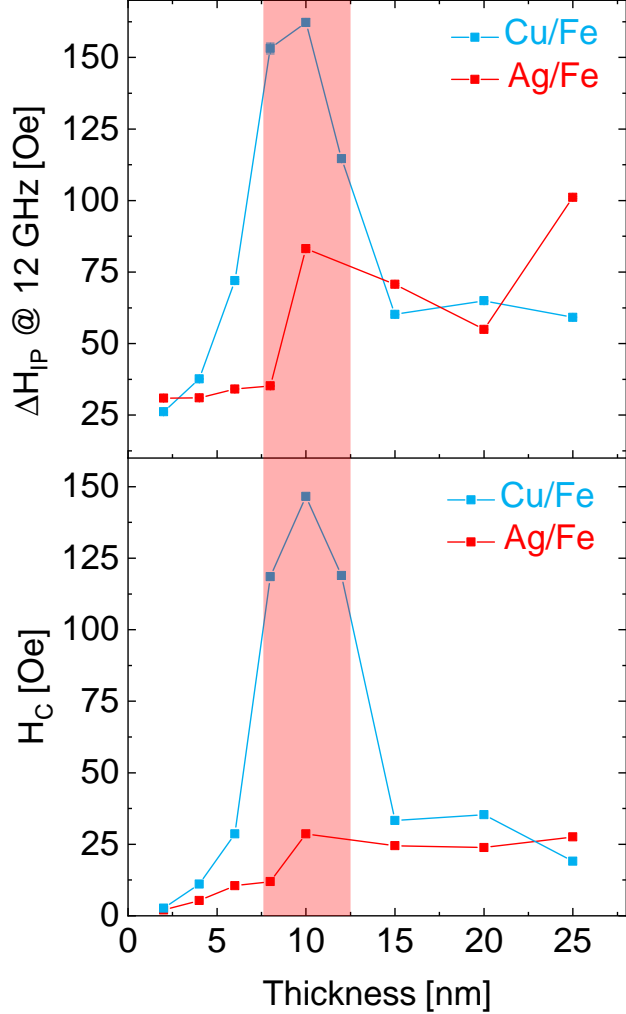


FIG. 5. (Color online) (a) IP FMR half-width-at-half-maximum linewidth at 12 GHz as a function of film thickness for both Cu/Fe and Ag/Fe. (b) Coercivity H_c as a function of film thickness for both Cu/Fe and Ag/Fe. The red shaded area highlights thickness region where the Cu/Fe sample series show a peak behavior in both plots.

magnon scattering here is not governed by the interfacial roughness of Fe films. The contrast between Cu/Fe and Ag/Fe also might appear counterintuitive, since two-magnon scattering is induced by defects and hence might be expected to be stronger for more “defective” films (i.e., Ag/Fe in this case). The counterintuitive nature of the two-magnon scattering here points to more subtle mechanisms at work.

To search for a possible correlation between static magnetic properties and two-magnon scattering, we have performed vibrating sample magnetometry (VSM) measurements with a Microsense EZ9 VSM. Coercivity extracted from VSM measurements is plotted as a function

of film thickness in Fig. 5(b), which shows a remarkably close correspondence with linewidth vs. thickness (Fig. 5(a)). In particular, a pronounced peak in coercivity is observed for Cu/Fe around 10 nm, corresponding to the same thickness regime where the 12 GHz FMR linewidth for Cu/Fe is maximized. Moreover, the 10 nm Cu/Fe sample (see Sec. II) exhibits a tall, narrow bcc (110) diffraction peak, which suggests that a larger crystal grain size plays a possible role in the large two-magnon scattering and coercivity (e.g., via stronger domain wall pinning).

While the trends shown in Fig. 5 provide some qualitative insights, we now attempt to quantitatively analyze the frequency dependence of FMR linewidth for the Cu/Fe and Ag/Fe films. We assume that the Gilbert damping parameter for IP FMR is equal to that for OOP FMR, i.e., $\alpha_{\text{IP}} = \alpha_{\text{OOP}}$. This assumption is physically reasonable, considering that Gilbert damping is theoretically expected to be isotropic in Fe films near room temperature⁴⁰. While a recent study has reported anisotropic Gilbert damping that scales quadratically with magnetostriction⁴⁶, this effect is likely negligible in elemental Fe whose magnetostriction is several times smaller^{47,48} than that of the Fe_{0.7}Ga_{0.3} alloy in Ref.⁴⁶.

Thus, from the measured IP linewidth ΔH_{IP} , the extrinsic two-magnon scattering linewidth ΔH_{TMS} can be obtained by

$$\Delta H_{\text{TMS}} = \Delta H_{\text{IP}} - \frac{2\pi}{\gamma} \alpha_{\text{IP}}, \quad (2)$$

where $\frac{2\pi}{\gamma} \alpha_{\text{IP}}$ is the Gilbert damping contribution. Figure 6 shows the obtained ΔH_{TMS} and fit attempts using the “grain-to-grain” two-magnon scattering model developed by McMicheal and Krivosik²⁵. This model captures the inhomogeneity of the effective internal magnetic field in a film consisting of many magnetic grains. The magnetic inhomogeneity can arise from the distribution of magnetocrystalline anisotropy field directions associated with the randomly oriented crystal grains⁴³. In this model the two-magnon scattering linewidth ΔH_{TMS} is a function of the Gilbert damping parameter α_{IP} , the effective anisotropy field H_a of the randomly oriented grain, and the correlation length ξ within which the effective internal magnetic field is correlated. Further details for computing ΔH_{TMS} are provided in the Appendix and Refs.^{25,43,44}. As we have specified above, the value of α_{IP} is set to the value derived from OOP FMR results (i.e., α_{OOP} in Fig. 3(b)). This leaves ξ and H_a as the only free parameters in the fitting process.

The modeling results are dependent on the choice of the correlation function $C(\mathbf{R})$, which

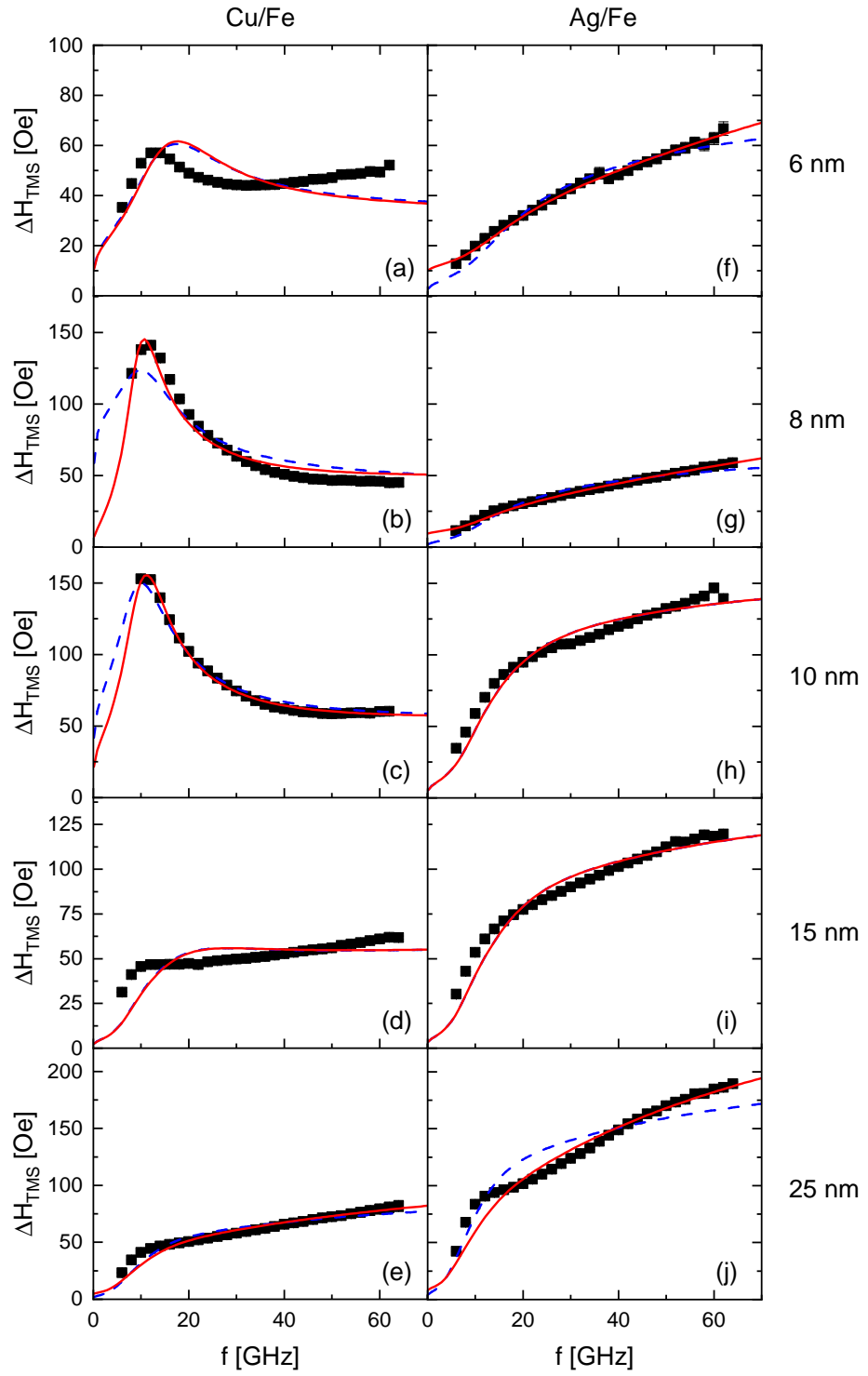


FIG. 6. (Color online) Extrinsic two-magnon scattering linewidth vs frequency and fitted curves for 6, 8, 10, 15, and 25 nm Cu/Fe and Ag/Fe films. Black squares represent experimental FMR linewidth data. Dashed blue and solid red curves represent the fitted curves using correlation functions proposed for modeling self-affine and mounded surfaces, respectively. In (d), (e), (h), (i), dashed blue curves overlap with solid red curves.

captures how the effective internal magnetic field is correlated as a function of lateral distance \mathbf{R} in the film plane. We first show results obtained with a simple exponentially decaying correlation function, as done in prior studies of two-magnon scattering^{25,43,44}, i.e.,

$$C(\mathbf{R}) = \exp\left(-\frac{|\mathbf{R}|}{\xi}\right). \quad (3)$$

Equation 3 has the same form as the simplest correlation function used to model rough topographical surfaces (when they are assumed to be “self-affine”)⁴⁹. Fit results with Eq. (3) are shown in dashed blue curves in Fig. 6. For most samples, the fitted curve does not reproduce the experimental data quantitatively. Moreover, the fitted values of ξ and H_a often reach physically unrealistic values, e.g., with H_a diverging to $> 10^4$ Oe and $\xi < 1$ nm (see Table I). These results suggest that the model does not properly capture the underlying physics of two-magnon scattering in our samples.

A possible cause for the failure to fit the data is that the simple correlation function is inadequate. We therefore consider an alternative correlation function by again invoking an analogy between the spatially varying height of a rough surface⁴⁹ and the spatially varying effective internal magnetic field in a film. Specifically, we apply a correlation function (i.e., a special case of Eq. (4.3) in Ref.⁴⁹ where short-range roughness $\alpha = 1$) for the so-called “mounded surface,” which incorporates the average distance λ between peaks in topographical height (or, analogously, effective internal magnetic field):

$$C(\mathbf{R}) = \frac{\sqrt{2}|\mathbf{R}|}{\xi} K_1\left(\frac{\sqrt{2}|\mathbf{R}|}{\xi}\right) J_0\left(\frac{2\pi|\mathbf{R}|}{\lambda}\right), \quad (4)$$

where J_0 and K_1 are the Bessel function of the first kind of order zero and the modified Bessel function of the second kind of order one, respectively. This oscillatory decaying function is chosen because its Fourier transform (see Appendix) does not contain any transcendental functions, which simplifies the numerical calculation. The fitted curves using the model with Eq. (4) are shown in solid red curves in Fig. 6. Fit results for some samples show visible improvement, although this is perhaps not surprising with the introduction of λ as an additional free parameter. Nevertheless, the fitted values of H_a or λ still diverge to unrealistic values of $> 10^4$ Oe or $> 10^4$ nm in some cases (see Table I), which means that the new correlation function (Eq. (4)) does not fully reflect the meaningful underlying physics of our sample either. More detailed characterization of the microstructure and inhomogeneities, e.g., via synchrotron x-ray and neutron scattering, could help determine

the appropriate correlation function. It is also worth pointing out that for some samples (e.g. 15 nm Cu/Fe and Ag/Fe films), essentially identical fit curves are obtained regardless of the correlation function. This is because when $\lambda \gg \xi$, the Fourier transform of Eq (4) has a very similar form as the Fourier transform of Eq (3), as shown in the Appendix. In such cases, the choice of the correlation function has almost no influence on the behavior of the two-magnon scattering model in the fitting process.

TABLE I. Summary of IP FMR linewidth fit results. Note the divergence to physically unreasonable values in many of the results. Standard error is calculated using equation $\sqrt{\text{SSR}/\text{DOF} \times \text{diag}(\text{COV})}$, where SSR stands for the sum of squared residuals, DOF stands for degrees of freedom, and **COV** stands for the covariance matrix.

Sample Series	Thickness (nm)	Self-affine		Mounded		
		ξ (nm)	H_a (Oe)	ξ (nm)	H_a (Oe)	λ (nm)
Cu/Fe	6	70 ± 10	170 ± 10	80 ± 90	24 ± 3	$>1 \times 10^4$
	8	200 ± 100	150 ± 20	700 ± 1000	25 ± 2	900 ± 100
	10	140 ± 40	200 ± 20	160 ± 50	33 ± 1	800 ± 200
	15	9 ± 2	800 ± 100	10 ± 20	100 ± 80	$>1 \times 10^4$
	25	0 ± 5	$>1 \times 10^4$	60 ± 30	$>1 \times 10^4$	10.41 ± 0.01
Ag/Fe	6	0 ± 40	$>1 \times 10^4$	150 ± 40	$>1 \times 10^4$	11.7 ± 0.7
	8	0 ± 30	$>1 \times 10^4$	170 ± 50	$>1 \times 10^4$	12 ± 4
	10	6 ± 1	1500 ± 300	8 ± 40	200 ± 500	$>1 \times 10^4$
	15	2 ± 2	4000 ± 3000	3 ± 9	500 ± 900	$>6 \times 10^3$
	25	0 ± 6	$>1 \times 10^4$	140 ± 50	$>1 \times 10^4$	15 ± 6

V. SUMMARY

We have examined intrinsic and extrinsic damping in two series of polycrystalline Fe thin films with distinct structural properties: (1) strongly textured, smooth Fe films grown on Cu and (2) weakly textured, rough Fe films grown on Ag. Out-of-plane FMR measurements confirm constant intrinsic Gilbert damping of ≈ 0.0024 , essentially independent of film thickness and structural properties. This finding implies that intrinsic damping in Fe may be

predominantly governed by the crystalline and electronic band structures within the grains, rather than scattering at grain boundaries or film surfaces. The results from in-plane FMR, where extrinsic damping (i.e., two-magnon scattering) plays a significant role, are far more nuanced. The conventional grain-to-grain two-magnon scattering model fails to reproduce the in-plane FMR linewidth data with physically reasonable parameters – pointing to the need to modify the model, along with more detailed characterization of the film microstructure. Our experimental findings advance the understanding of intrinsic Gilbert damping in polycrystalline Fe, while motivating further studies to uncover the mechanisms of extrinsic damping in structurally disordered thin films of the elemental ferromagnetic metal.

ACKNOWLEDGMENTS

S.W. acknowledges support by the ICTAS Junior Faculty Program. D.A.S. and S.E. acknowledge support by the National Science Foundation, Grant No. DMR-2003914. P. N. would like to acknowledge support through NASA Grant NASA CAN80NSSC18M0023. A. R. would like to acknowledge support through the Defense Advanced Research Project Agency (DARPA) program on Topological Excitations in Electronics (TEE) under Grant No. D18AP00011. This work was supported by NanoEarth, a member of National Nanotechnology Coordinated Infrastructure (NNCI), supported by NSF (ECCS 1542100).

Appendix A: Details of the Two-Magnon Scattering Model

In the model developed by McMichael and Krivosik, the two-magnon scattering contribution ΔH_{TMS} to the FMR linewidth is given by^{25,43,44}

$$\Delta H_{\text{TMS}} = \frac{\gamma^2 H_a^2}{2\pi P_A(\omega)} \int \Lambda_{0k} C_k(\xi) \delta_\alpha(\omega - \omega_k) d^2k \quad (\text{A1})$$

where ξ is correlation length, H_a is the effective anisotropy field of the randomly oriented grain. $P_A(\omega) = \frac{\partial\omega}{\partial H}|_{H=H_{\text{FMR}}} = \sqrt{1 + (\frac{4\pi M_s}{2\omega/\gamma})^2}$ accounts for the conversion between the frequency and field swept linewidth. Λ_{0k} represents the averaging of the anisotropy axis fluctuations over the sample. It also takes into account the ellipticity of the precession for both the uniform FMR mode and the spin wave mode⁴³. The detailed expression of Λ_{0k} can be found in the Appendix of Ref.⁴³. The coefficients in the expression of Λ_{0k} depend on

the type of anisotropy of the system. Here, we used first-order cubic anisotropy for bcc Fe. $\delta_\alpha(\omega - \omega_k)$ selects all the degenerate modes, where ω represents the FMR mode frequency and ω_k represents the spin wave mode frequency. The detailed expression of ω_k can be found in Ref.²⁵. In the ideal case where Gilbert damping is 0, δ_α is the Dirac delta function. For a finite damping, $\delta_\alpha(\omega_0 - \omega_k)$ is replaced by a Lorentzian function $\frac{1}{\pi} \frac{(\alpha_{\text{IP}}\omega_k/\gamma)\partial\omega/\partial H}{(\omega_k - \omega)^2 + [(\alpha_{\text{IP}}\omega_k/\gamma)\partial\omega/\partial H]^2}$, which centers at ω and has the width of $(2\alpha_{\text{IP}}\omega_k/\gamma)\partial\omega/\partial H$.

Finally, $C_k(\xi)$ (or $C_k(\xi, \lambda)$) is the Fourier transform of the grain-to-grain internal field correlation function, Eq. (3) (or Eq. (4)). For the description of magnetic inhomogeneity analogous to the simple self-affine topographical surface⁴⁹, the Fourier transform of the correlation function, Eq. (3), is

$$C_k(\xi) = \frac{2\pi\xi^2}{[1 + (k\xi)^2]^{\frac{3}{2}}}, \quad (\text{A2})$$

as also used in Refs.^{25,43,44}. For the description analogous to the mounded surface, the Fourier transform of the correlation function, Eq. (4), is⁴⁹

$$C_k(\xi, \lambda) = \frac{8\pi^3\xi^2 \left(1 + \frac{2\pi^2\xi^2}{\lambda^2} + \frac{\xi^2}{2}k^2\right)}{\left[\left(1 + \frac{2\pi^2\xi^2}{\lambda^2} + \frac{\xi^2}{2}k^2\right)^2 - \left(\frac{2\pi\xi^2}{\lambda}k\right)^2\right]^{3/2}}. \quad (\text{A3})$$

When $\lambda \gg \xi$, Eq. (A3) becomes

$$C_k(\xi) \approx \frac{8\pi^3\xi^2}{\left(1 + \frac{\xi^2}{2}k^2\right)^2}, \quad (\text{A4})$$

which has a similar form as Eq. (A2). This similarity can also be demonstrated graphically. Figure 7 plots a self-affine C_k curve (Eq. (A2)) at $\xi = 100$ nm and three mounded C_k curves (Eq. (A3)) at $\lambda = 10, 100, 1000$ nm. ξ in mounded C_k curves is set as 100 nm as well. It is clearly shown in Fig. 7 that when $\lambda = 1000$ nm, the peak appearing in $\lambda = 10$ and 100 nm mounded C_k curves disappears and the curve shape of mounded C_k resembles that of self-affine C_k .

¹ Z. Diao, Z. Li, S. Wang, Y. Ding, A. Panchula, E. Chen, L.-C. Wang, and Y. Huai, J. Phys. Condens. Matter **19**, 165209 (2007).

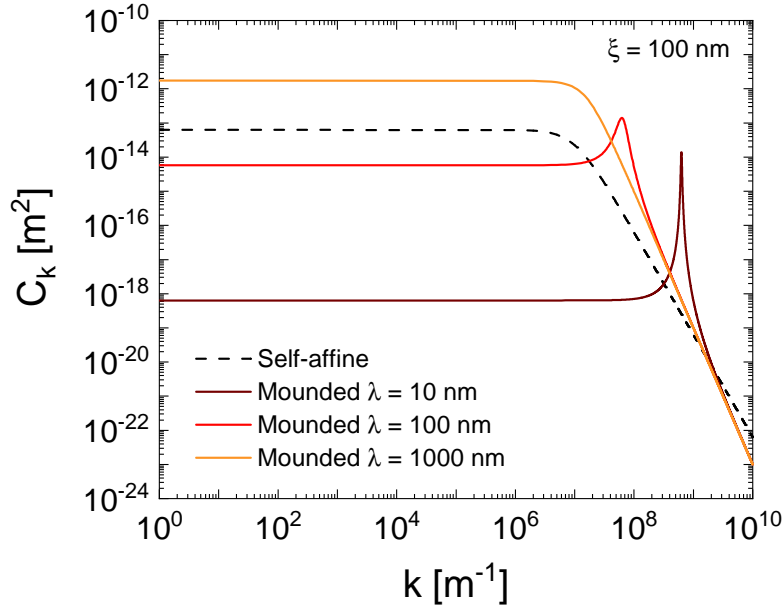


FIG. 7. Fourier transform of correlation function for mounded surfaces as a function of k for three different λ values. Fourier transform of correlation function for self-affine surfaces as a function of k is also included for comparison purpose. ξ is set as 100 nm for all curves.

- ² X. Zhu and J.-G. Zhu, IEEE Transactions on Magnetics **43**, 2349 (2007).
- ³ H. Yu, O. d'Allivy Kelly, V. Cros, R. Bernard, P. Bortolotti, A. Anane, F. Brandl, R. Huber, I. Stasinopoulos, and D. Grundler, Sci. Rep. **4** (2014), 10.1038/srep06848.
- ⁴ G. E. Rowlands, C. A. Ryan, L. Ye, L. Rehm, D. Pinna, A. D. Kent, and T. A. Ohki, Sci. Rep. **9** (2019), 10.1038/s41598-018-37204-3.
- ⁵ I. Kanada, A. Cruce, T. Mewes, S. Wu, C. Mewes, G. Mankey, and T. Suzuki, AIP Adv. **7**, 056105 (2017).
- ⁶ S. S. P. Parkin, C. Kaiser, A. Panchula, P. M. Rice, B. Hughes, M. Samant, and S.-H. Yang, Nat. Mater. **3**, 862 (2004).
- ⁷ Y. Ando, T. Miyakoshi, M. Oogane, T. Miyazaki, H. Kubota, K. Ando, and S. Yuasa, Appl. Phys. Lett. **87**, 142502 (2005).
- ⁸ T. L. Gilbert, Phys. Rev., **100**, 1243 (1955).
- ⁹ T. Gilbert, IEEE Transactions on Magnetics **40**, 3443 (2004).
- ¹⁰ B. Heinrich, D. Fraitová, and V. Kamberský, Phys. Status Solidi B **23**, 501 (1967).
- ¹¹ V. Kamberský, Czech. J. Phys. **26**, 1366 (1976).

¹² Y. Tserkovnyak, G. A. Fiete, and B. I. Halperin, *Appl. Phys. Lett.* **84**, 5234 (2004).

¹³ E. Rossi, O. G. Heinonen, and A. H. MacDonald, *Phys. Rev. B* **72**, 174412 (2005).

¹⁴ M. A. W. Schoen, D. Thonig, M. L. Schneider, T. J. Silva, H. T. Nembach, O. Eriksson, O. Karis, and J. M. Shaw, *Nat. Phys.* **12**, 839 (2016).

¹⁵ K. Gilmore, Y. U. Idzerda, and M. D. Stiles, *Phys. Rev. Lett.* **99**, 027204 (2007).

¹⁶ S. Mankovsky, D. Ködderitzsch, G. Woltersdorf, and H. Ebert, *Phys. Rev. B* **87**, 014430 (2013).

¹⁷ Eddy-current damping⁵⁰ and radiative damping³⁵ can also contribute to viscous damping, but they typically constitute a small correction that is $\lesssim 10\%$ of intrinsic Gilbert damping in ferromagnetic thin films (i.e., $\lesssim 20$ nm thick) for nanomagnetic devices^{18,34}, which are thought to be rooted in the electronic band structure of the ferromagnetic metal^{14–16}.

¹⁸ B. Khodadadi, A. Rai, A. Sapkota, A. Srivastava, B. Nepal, Y. Lim, D. A. Smith, C. Mewes, S. Budhathoki, A. Hauser, M. Gao, J.-F. Li, D. Viehland, Z. Jiang, J. Heremans, P. Balachandran, T. Mewes, and S. Emori, *Phys. Rev. Lett.* **124**, 157201 (2020).

¹⁹ S. Geschwind and A. M. Clogston, *Phys. Rev.* **108**, 49 (1957).

²⁰ R. C. LeCraw, E. G. Spencer, and C. S. Porter, *Phys. Rev.* **110**, 1311 (1958).

²¹ E. Schlömann, *J. Phys. Chem. Solids* **6**, 257 (1958).

²² C. E. Patton, C. H. Wilts, and F. B. Humphrey, *J. Appl. Phys.* **38**, 1358 (1967).

²³ R. Arias and D. L. Mills, *Phys. Rev. B* **60**, 7395 (1999).

²⁴ R. Arias and D. L. Mills, *J. Appl. Phys.* **87**, 5455 (2000).

²⁵ R. McMichael and P. Krivosik, *IEEE Transactions on Magnetics* **40**, 2 (2004).

²⁶ G. Woltersdorf and B. Heinrich, *Phys. Rev. B* **69**, 184417 (2004).

²⁷ N. Mo, Y.-Y. Song, and C. E. Patton, *J. Appl. Phys.* **97**, 093901 (2005).

²⁸ S. S. Kalarickal, N. Mo, P. Krivosik, and C. E. Patton, *Phys. Rev. B* **79**, 094427 (2009).

²⁹ J. Lindner, I. Barsukov, C. Raeder, C. Hassel, O. Posth, R. Meckenstock, P. Landeros, and D. L. Mills, *Phys. Rev. B* **80**, 224421 (2009).

³⁰ S. Jiang, L. Sun, Y. Yin, Y. Fu, C. Luo, Y. Zhai, and H. Zhai, *AIP Adv.* **7**, 056029 (2017).

³¹ E. R. Edwards, H. T. Nembach, and J. M. Shaw, *Phys. Rev. Appl.* **11**, 054036 (2019).

³² G. Vignaud and A. Gibaud, *J. Appl. Crystallogr.* **52**, 201 (2019).

³³ Here, the “average roughness” is the average of the roughness of the top and bottom interfaces of the Fe layer.

³⁴ D. A. Smith, A. Rai, Y. Lim, T. Q. Hartnett, A. Sapkota, A. Srivastava, C. Mewes, Z. Jiang,

M. Clavel, M. K. Hudait, D. D. Viehland, J. J. Heremans, P. V. Balachandran, T. Mewes, and S. Emori, Phys. Rev. Appl **14**, 034042 (2020).

³⁵ M. A. W. Schoen, J. M. Shaw, H. T. Nembach, M. Weiler, and T. J. Silva, Phys. Rev. B **92**, 184417 (2015).

³⁶ B. Heinrich, K. B. Urquhart, A. S. Arrott, J. F. Cochran, K. Myrtle, and S. T. Purcell, Phys. Rev. Lett. **59**, 1756 (1987).

³⁷ Z. Celinski and B. Heinrich, J. Appl. Phys. **70**, 5935 (1991).

³⁸ K. Gilmore, *Precession damping in itinerant ferromagnets*, Ph.D. thesis, Montana State University-Bozeman, College of Letters & Science (2007).

³⁹ G. S. Abo, Y.-K. Hong, J. Park, J. Lee, W. Lee, and B.-C. Choi, IEEE Transactions on Magnetics **49**, 4937 (2013).

⁴⁰ K. Gilmore, M. D. Stiles, J. Seib, D. Steiauf, and M. Fähnle, Phys. Rev. B **81**, 174414 (2010).

⁴¹ J. T. Hou and L. Liu, Phys. Rev. Lett. **123**, 107702 (2019).

⁴² Y. Li, T. Polakovic, Y.-L. Wang, J. Xu, S. Lendinez, Z. Zhang, J. Ding, T. Khaire, H. Saglam, R. Divan, J. Pearson, W.-K. Kwok, Z. Xiao, V. Novosad, A. Hoffmann, and W. Zhang, Phys. Rev. Lett. **123**, 107701 (2019).

⁴³ S. S. Kalarickal, P. Krivosik, J. Das, K. S. Kim, and C. E. Patton, Phys. Rev. B **77**, 054427 (2008).

⁴⁴ W. K. Peria, T. A. Peterson, A. P. McFadden, T. Qu, C. Liu, C. J. Palmstrøm, and P. A. Crowell, Phys. Rev. B **101**, 134430 (2020).

⁴⁵ A. Azevedo, A. B. Oliveira, F. M. de Aguiar, and S. M. Rezende, Phys. Rev. B **62**, 5331 (2000).

⁴⁶ W. K. Peria, X. Wang, H. Yu, S. Lee, I. Takeuchi, and P. A. Crowell, Phys. Rev. B **103**, L220403 (2021).

⁴⁷ A. E. Clark, K. B. Hathaway, M. Wun-Fogle, J. B. Restorff, T. A. Lograsso, V. M. Keppens, G. Petculessu, and R. A. Taylor, J. Appl. Phys. **93**, 8621 (2003).

⁴⁸ E. M. Summers, T. A. Lograsso, and M. Wun-Fogle, J Mater Sci **42**, 9582 (2007).

⁴⁹ M. Pelliccione and T.-M. Lu, in *Springer Series in Materials Science*, Vol. 108 (Springer, 2008).

⁵⁰ C. Scheck, L. Cheng, and W. E. Bailey, Appl. Phys. Lett. **88**, 252510 (2006).